AIAA JOURNAL
Vol. 33, No. 9, September 1995

Sensitivity Analysis of Unsteady Aerodynamic Loads in Cascades

Christopher B. Lorence* and Kenneth C. Hall†
Duke University, Durham, North Carolina 27708-0300

A method for computing the effect perturbations in the shape of airfoils in a cascade have on the steady and unsteady flow through the cascade is presented. First, the full potential equation is used to describe the behavior of the nonlinear steady flow and the small disturbance unsteady flow through the cascade. The steady flow and small disturbance unsteady flow versions of the full potential equation are then discretized on a computational grid of quadrilateral cells using a variational finite element technique. The resulting discretized equations describing the nonlinear steady flow are solved using Newton iteration with lower–upper decomposition at each iteration. Similarly, the discretized unsteady small disturbance equations, which are linear, are solved using a single lower–upper decomposition. Next, a sensitivity analysis is performed to determine the effect small changes in cascade and airfoil geometry have on the steady and unsteady flowfields. The sensitivity analysis makes use of the nominal steady and unsteady flow lower–upper decompositions so that no additional matrices need to be factored. Hence, the present method is computationally very efficient. A number of cases are presented in the paper to show the accuracy of the present method. We also demonstrate how the sensitivity analysis may be used to redesign a representative compressor cascade for improved aeroelastic stability.

Introduction

As the efficiency of modern aircraft engines continues to increase, aeroelastic considerations play an increasingly important role in the design of turbomachinery blading. Currently, however, the steady aerodynamic design and the aeroelastic design phases during the development of fan, compressor, and turbine blading are largely decoupled. First, the blade is designed primarily to maximize steady aerodynamic performance. Then, detailed aeroelastic studies are performed to determine whether the blades will meet standards for flutter stability and fatigue. If the blade fails to meet these requirements, the blade is redesigned, and the process is repeated. This redesign process increases the time and expense required to design a blade and misses an opportunity to simultaneously design for steady and unsteady aerodynamic performance.

In recent years, the capability to analyze unsteady flows in cascades has substantially improved. For example, a number of linearized analyses of unsteady flows about loaded airfoils have been developed. These include potential analyses,[1,2] potential analyses with vortical gust effects,[3,4] and linearized Euler analyses.[5–8] However, these linearized flow models are best viewed as analysis tools rather than design tools. They are capable of solving the direct problem where the shape of the airfoil as well as the flow conditions are specified. Unfortunately, except through trial and error or extensive parametric studies, these codes do not provide physical insight into how to design cascades to be aeroelastically stable.

A substantial body of work exists on the inverse design and optimal design of airfoils.[9–12] Most of this work, however, is directed at achieving desirable steady flow properties. Researchers have also developed aeroelastic optimization techniques for rotorcraft,[13] aircraft,[14] and turbomachinery.[15] These analyses have focused primarily on structural optimization rather than optimization of the unsteady aerodynamic behavior.

One of the key ingredients in optimization algorithms is the evaluation of the sensitivity of the quantity to be optimized (for example, the flutter stability or efficiency of a cascade) to a small change in a physical parameter (such as the airfoil shape). Sensitivity analysis of structures has been an active area of research for the past decade.[16,17] Recently, researchers have begun to develop similar sensitivity analysis techniques for steady aerodynamic problems. For example, Taylor et al.[18] and Baysal and Eleshaky[19] have computed the effect of modifying the shape of a nozzle on the flow in the nozzle. Their work was based on a sensitivity analysis of the discretized Euler equations. Most recently, such techniques have been applied to airfoil design.[20] Despite these advances, only a few unsteady aerodynamic sensitivity analyses have been reported in the literature, for example, the semianalytical panel method of Murthy and Kaza.[21] Other unsteady aerodynamic sensitivity analyses have been performed by numerically differencing two unsteady flow solutions computed for slightly different values of some physical parameter. The use of finite difference sensitivity analyses, however, is less desirable than an analytical method because of the large computational expense and susceptibility to round-off and truncation errors associated with finite difference techniques.

In this paper, we present a new method for computing the sensitivity of steady and unsteady flows in cascades to small changes in airfoil and cascade geometry. The nominal steady and unsteady flows are computed using a full potential solver based on a deforming grid variational principle and finite element method developed by Hall.[22] To calculate the sensitivities, a perturbation analysis is performed on the nominal steady and unsteady finite element equations. This leads to a set of linear matrix equations for the sensitivity of the steady and unsteady potential due to small changes in the airfoil shape. The matrix equations to be solved are the same as the nominal flow matrix equations but with new right-hand sides. Thus, if the nominal flows have been computed using lower–upper (LU) decomposition, then no additional matrices need to be factored, and the sensitivities can be computed by back substitution. Consequently, the sensitivity of the steady and unsteady potentials can be computed very efficiently.

Theory

Nominal Flowfield Description

In the present analysis, the flow through a blade row is assumed to be inviscid, isentropic, irrotational, and two dimensional. In addition, the fluid is assumed to be an ideal gas with constant specific heats. Thus, the velocity field may be represented by the gradient of a scalar potential $\hat{\phi}$. This potential satisfies the unsteady full potential equation

$$\nabla^2\hat{\phi} = \frac{1}{\hat{c}^2}\left[\frac{\partial^2\hat{\phi}}{\partial t^2} + 2\nabla\hat{\phi}\cdot\nabla\frac{\partial\hat{\phi}}{\partial t} + \frac{1}{2}\nabla\hat{\phi}\cdot\nabla(\nabla\hat{\phi})^2\right] \quad (1)$$

Presented as Paper 94-0064 at the AIAA 32nd Aerospace Sciences Meeting, Reno, NV, Jan. 10–13, 1994; received Jan. 14, 1994; revision received Feb. 7, 1995; accepted for publication Feb. 7, 1995.

*Graduate Research Assistant, Department of Mechanical Engineering and Materials Science. Member AIAA.

†Assistant Professor, Department of Mechanical Engineering and Materials Science. Member AIAA.

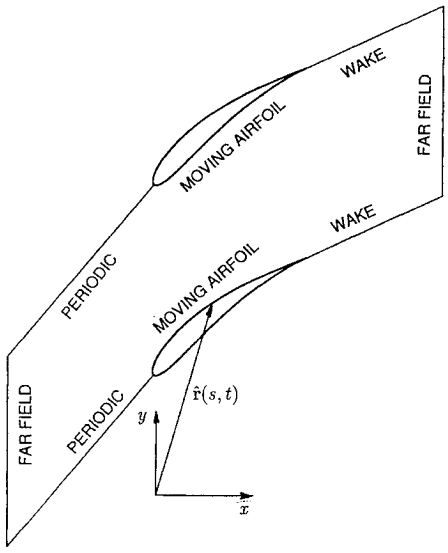

Fig. 1 Typical solution domain used for calculation of flow through cascades.

where $\hat{c}$ is the local speed of sound. The static pressure and density may be expressed in terms of the velocity potential, i.e.,

$$\hat{p} = p_T\left\{1 - \frac{\gamma - 1}{C_T^2}\left[\frac{1}{2}(\nabla\hat{\phi})^2 + \frac{\partial\hat{\phi}}{\partial t}\right]\right\}^{\gamma/(\gamma-1)} \tag{2}$$

$$\hat{\rho} = \rho_T\left\{1 - \frac{\gamma - 1}{C_T^2}\left[\frac{1}{2}(\nabla\hat{\phi})^2 + \frac{\partial\hat{\phi}}{\partial t}\right]\right\}^{1/(\gamma-1)} \tag{3}$$

where p_T is the total pressure, ρ_T the total density, and C_T the total speed of sound. Equation (2) is simply the unsteady Bernoulli equation.

To complete the problem specification, boundary conditions must be specified around the boundaries of the computational domain, in this case, a single blade passage (see Fig. 1). The five main boundary types are moving airfoil, upstream periodic, downstream periodic/wake, upstream far-field, and downstream far-field boundaries. On airfoil surfaces, the boundary condition is that there can be no mass flux through the airfoil so that

$$\nabla\hat{\phi}\cdot\hat{\boldsymbol{n}} = \frac{\partial\hat{\boldsymbol{r}}}{\partial t}\cdot\hat{\boldsymbol{n}} \tag{4}$$

where $\hat{\boldsymbol{n}}$ is the unit normal to the airfoil surface, and the surface of the airfoil at any time t is described by the parameterized position vector $\hat{\boldsymbol{r}}$. Similarly, the wake is considered to be an impermeable surface so that Eq. (4) also applies on both sides of the wake, but now $\hat{\boldsymbol{r}}$ is the unknown displacement of the wake. Also, the pressure jump across the wake must be zero. Periodic boundary conditions are applied along the upstream and downstream periodic boundaries to reduce the computational domain to a single blade passage. Finally, for unsteady flow problems, nonreflecting boundary conditions must be applied on the upstream and downstream far-field boundaries to prevent spurious reflections of outgoing waves.

The problem of solving for the unsteady flow in the cascade is divided into two parts. First, we solve for the nonlinear steady flow through the cascade. Next, we assume that the unsteadiness in the flow is a small harmonic disturbance about the steady flow with temporal frequency ω. Therefore, the unsteady perturbation flow can be described by a set of linear variable coefficient equations.

To increase the accuracy of the unsteady solution procedure, the unsteady velocity potential is computed on a deforming computational grid which conforms to the motion of the moving airfoils. We define two coordinate systems. The first coordinate system (x, y, t) is the usual physical coordinate system. The second coordinate system (ξ, η, τ) is the computational coordinate system that is "attached" to the computational grid, that is, the grid is stationary with respect to the computational coordinates. Thus, a grid point fixed in the computational coordinate system (ξ, η, τ) moves in the physical coordinate system (x, y, t) as the grid deforms. Because the motion of airfoils (and, hence, the grid) is small, the two coordinate systems only differ by a small perturbation, i.e.,

$$x(\xi, \eta, \tau) = \xi + f(\xi, \eta)e^{j\omega\tau} \tag{5}$$

$$y(\xi, \eta, \tau) = \eta + g(\xi, \eta)e^{j\omega\tau} \tag{6}$$

$$t(\xi, \eta, \tau) = \tau \tag{7}$$

where f and g are the complex amplitudes of the small perturbations describing the grid motion in the x and y directions. The functions f and g are chosen so that the motion of the grid along the airfoil boundary conforms to the motion of the airfoils, and the motion of the grid satisfies complex periodicity along the upstream and downstream periodic boundaries. Note that to zeroth order, the physical and computational coordinate systems are identical.

Similarly, the velocity potential is expanded in a perturbation series of the form

$$\hat{\phi}(\xi, \eta, \tau) = \Phi(\xi, \eta) + \phi(\xi, \eta)e^{j\omega\tau} \tag{8}$$

where Φ and ϕ are the steady flow and small disturbance unsteady velocity potentials, respectively. Substitution of Eqs. (5–8) into the full potential equation, Eq. (1), and collection of terms of zeroth and first order gives the steady flow and small disturbance flow equations. The steady flow potential equation is given by

$$\nabla^2\Phi = (1/C^2)\left[\tfrac{1}{2}\nabla\Phi\cdot\nabla(\nabla\Phi)^2\right] \tag{9}$$

where C is the local steady speed of sound and is a function of the steady potential Φ. Note that Eq. (9) is nonlinear in the unknown potential Φ.

The small disturbance unsteady potential equation is given by

$$\nabla'\cdot R\nabla'\phi - \nabla'\cdot[R/C^2(\nabla'\Phi^T\nabla'\phi + j\omega\phi)\nabla'\Phi]$$
$$-(R/C^2)(j\omega\nabla'\Phi^T\nabla'\phi - \omega^2\phi) = b \tag{10}$$

where b is an inhomogeneous term that is a function of the computed steady flow and the prescribed grid motion (see Ref. 22), and R is the steady flow density. Here ∇' is the gradient in the (ξ, η) coordinate system, i.e., $\nabla = \boldsymbol{J}\nabla'$, where $\boldsymbol{J}$ is the Jacobian of the coordinate transformation. The small disturbance equation is seen to be linear in the unsteady potential ϕ with coefficients that depend on the nonlinear steady flow potential Φ.

In a completely analogous fashion, the boundary conditions may be split into steady flow and small disturbance flow parts. Steady flow and small disturbance flow boundary conditions must be specified at the inflow, outflow, periodic, and wake boundaries. For brevity, the details of these boundary conditions are omitted. We note, however, that the far-field boundary conditions for the unsteady flow solver are analytically exact nonreflecting boundary conditions based on the behavior of the linearized full potential equation in the far field.[23] The remaining boundary conditions are substantially the same as described in Ref. 22.

Once one has solved for the steady and small disturbance potentials, one can compute the resulting steady pressure P and unsteady pressure p using the Bernoulli equation. Expanding Eq. (2) in a perturbation series, and collecting zeroth-order terms, one finds that the steady pressure P is given by

$$P = p_T\left\{1 - \left[(\gamma - 1)/2C_T^2\right](\nabla\Phi)^2\right\}^{\gamma/(\gamma-1)} \tag{11}$$

Similarly, collection of the first-order terms gives the unsteady pressure p,

$$p = -R\left[\nabla'\Phi^T\nabla'\phi + j\omega\phi - j\omega\boldsymbol{f}\cdot\nabla'\Phi + \tfrac{1}{2}\nabla'\Phi^T\tilde{\boldsymbol{J}}\nabla'\Phi\right] \tag{12}$$

where $\tilde{\boldsymbol{J}} = \boldsymbol{J}^T\boldsymbol{J} - \boldsymbol{I}$, and $\boldsymbol{f}$ is the vector of grid motion functions $(f, g)^T$. Finally, having computed the unsteady surface pressure, one can compute the unsteady lift and moment acting on the airfoil by performing appropriate integrations of the pressure around the surface of the airfoil.

Numerical Solution Technique

One could solve the given partial differential equations in a number of ways, e.g., using finite difference, finite volume, or finite element techniques. In the present analysis, we discretize these equations using a variational finite element technique. Hall[22] has shown that Eqs. (9) and (10) are the Euler–Lagrange equations of steady flow and small disturbance unsteady flow variational principles based on a variational principle due to Bateman.[24] Furthermore, the natural boundary condition of the variational principles are the steady and small disturbance no through flow conditions.

Consider the solution of the steady flow problem. First, an H grid, generated using an elliptic grid generation technique based on the work of Thompson et al.,[25] is used to subdivide the computational domain into a number of quadrilateral elements. Then, the steady flow variational principle is discretized on this computational grid using four-node isoparametric finite elements. The auxiliary boundary conditions are discretized using a combination of finite element and finite difference techniques (the auxiliary boundary conditions are boundary conditions which are not Dirichlet boundary conditions or natural boundary conditions of the variational principle). The result is a set of nonlinear equations of the form

$$\boldsymbol{N}(\boldsymbol{V};\boldsymbol{X}) = \boldsymbol{0} \tag{13}$$

where $\boldsymbol{N}$ is a vector of nonlinear functions, $\boldsymbol{V}$ the vector containing the as yet unknown steady velocity potential Φ at each of the computational nodes, and $\boldsymbol{X}$ a vector containing the location of the computational nodes (thus the airfoil shape is also contained in $\boldsymbol{X}$).

To solve Eq. (13) for the nominal airfoil and cascade geometry, we use Newton iteration. Hence, given the nth estimate of the solution $\boldsymbol{V}^n$ the $(n+1)$st estimate is given by

$$\boldsymbol{V}^{n+1} = \boldsymbol{V}^n - \left[\frac{\partial \boldsymbol{N}}{\partial \boldsymbol{V}}\right]_n^{-1} \boldsymbol{N}(\boldsymbol{V}^n, \boldsymbol{X}) \tag{14}$$

Thus, using Newton iteration, the system of nonlinear equations, Eq. (13), is reduced to a sequence of linear equations, Eq. (14). Because we use an H grid in the present investigation, the matrix $\partial \boldsymbol{N}/\partial \boldsymbol{V}$ is block tridiagonal. Of course the matrix in Eq. (14) is not actually inverted, but rather factored using an LU decomposition algorithm which takes advantage of the block-tridiagonal structure. The Newton iteration procedure is very fast with solutions typically obtained in about five iterations.

Having computed the nominal steady solution, we next discretize and solve the nominal linearized unsteady flow problem. The small disturbance variational principle is discretized, again using quadrilateral isoparametric finite elements, and the auxiliary equations are discretized using a combination of finite elements and finite difference operators. The result is a linear matrix equation of the form

$$\boldsymbol{A}\boldsymbol{v} = \boldsymbol{b} \tag{15}$$

where

$$\boldsymbol{A} = \boldsymbol{A}(\boldsymbol{V}, \boldsymbol{X}, \omega) \qquad \boldsymbol{b} = \boldsymbol{b}(\boldsymbol{V}, \boldsymbol{X}, \boldsymbol{f}, \omega)$$

and where $\boldsymbol{v}$ is the vector containing the nodal values of the unknown unsteady velocity potential ϕ. The matrix in Eq. (15) is large, sparse, complex, and block tridiagonal; Eq. (15) is solved efficiently using LU decomposition.

Sensitivity Analysis

Having computed the nominal steady and unsteady flowfields, we next determine the effect a small change in airfoil or cascade geometry has on the steady and unsteady flow. Returning to Eq. (13), if the geometry is perturbed slightly, the perturbed solution will satisfy the equation

$$\boldsymbol{N}(\boldsymbol{V}+\boldsymbol{V}';\boldsymbol{X}+\boldsymbol{X}') = \boldsymbol{0} \tag{16}$$

where $\boldsymbol{X}$ is the nominal grid (and, hence, cascade) geometry, $\boldsymbol{X}'$ is the perturbation in the geometry, $\boldsymbol{V}$ contains the nominal steady velocity potential, and $\boldsymbol{V}'$ is the sensitivity of the steady potential to perturbations in the geometry. Expanding Eq. (16) in a perturbation series about the nominal solution gives

$$\left[\frac{\partial \boldsymbol{N}}{\partial \boldsymbol{V}}\right]\boldsymbol{V}' + \left[\frac{\partial \boldsymbol{N}}{\partial \boldsymbol{X}}\right]\boldsymbol{X}' = \boldsymbol{0} \tag{17}$$

Therefore, solving for the unknown perturbation $\boldsymbol{V}'$ gives

$$\boldsymbol{V}' = -\left[\frac{\partial \boldsymbol{N}}{\partial \boldsymbol{V}}\right]^{-1}\left[\frac{\partial \boldsymbol{N}}{\partial \boldsymbol{X}}\right]\boldsymbol{X}' \tag{18}$$

Computationally, $[\partial \boldsymbol{N}/\partial \boldsymbol{X}]\boldsymbol{X}'$ is very inexpensive to form. Furthermore, note the similarity of Eq. (18) to Eq. (14). The same matrix must be "inverted" to obtain the perturbed steady solution that was used in the last iteration of the Newton solver. Therefore, if the steady flow has been computed using Newton iteration with LU decomposition and the last factored matrix has been saved, then the sensitivity $\boldsymbol{V}'$ can be obtained with very little additional computational work.

Having computed the sensitivity of the steady potential to a change in geometry, it is now possible to compute the resulting sensitivity of the unsteady potential. The solution of the unsteady flow problem due to small changes in the geometry, frequency, and mode shape will be of the form

$$[\boldsymbol{A}(\boldsymbol{V}+\boldsymbol{V}', \boldsymbol{X}+\boldsymbol{X}', \omega+\omega')]\{\boldsymbol{v}+\boldsymbol{v}'\} = \{\boldsymbol{b}(\boldsymbol{V}+\boldsymbol{V}', \boldsymbol{X}+\boldsymbol{X}', \boldsymbol{f}+\boldsymbol{f}', \omega+\omega')\} \tag{19}$$

where $\boldsymbol{f}'$ is the prescribed perturbation in the motion of the airfoil and grid, ω' the prescribed perturbation in the frequency of the unsteady motion, and $\boldsymbol{v}'$ the unknown sensitivity of the unsteady potential. Expanding Eq. (19) in a perturbation series and collecting terms of first order in $\boldsymbol{v}'$ gives

$$\boldsymbol{A}\boldsymbol{v}' = \left[\frac{\partial \boldsymbol{b}}{\partial \boldsymbol{V}}\right]\boldsymbol{V}' + \left[\frac{\partial \boldsymbol{b}}{\partial \boldsymbol{X}}\right]\boldsymbol{X}' + \left[\frac{\partial \boldsymbol{b}}{\partial \boldsymbol{f}}\right]\boldsymbol{f}' + \left[\frac{\partial \boldsymbol{b}}{\partial \omega}\right]\omega' - \left(\left[\frac{\partial \boldsymbol{A}}{\partial \boldsymbol{V}}\right]\boldsymbol{V}' + \left[\frac{\partial \boldsymbol{A}}{\partial \boldsymbol{X}}\right]\boldsymbol{X}' + \left[\frac{\partial \boldsymbol{A}}{\partial \omega}\right]\omega'\right)\boldsymbol{v} \tag{20}$$

or, more succinctly,

$$\boldsymbol{A}\boldsymbol{v}' = \boldsymbol{b}' - \boldsymbol{A}'\boldsymbol{v} \tag{21}$$

Here the terms $\boldsymbol{X}'$, $\boldsymbol{f}'$, and ω' are prescribed, and $\boldsymbol{V}'$ is known from the solution of the steady sensitivity problem.

There is a subtlety in the foregoing analysis. The steady flow is $\mathcal{O}(1)$; the leading order behavior of the unsteady flow is $\mathcal{O}(\epsilon_1)$ where ϵ_1 is the order of the blade displacement. Similarly, if the perturbation in the cascade geometry is $\mathcal{O}(\epsilon_2)$, then to leading order the change in the steady flow will be $\mathcal{O}(\epsilon_2)$. What then is the leading-order behavior in the unsteady flow due to changes in blade geometry? Clearly, the unsteady flowfield will be $\mathcal{O}(\epsilon_1\epsilon_2, \epsilon_1^2, \epsilon_1\epsilon_2^2, \epsilon_1^2\epsilon_2, \ldots)$. Since ϵ_1 and ϵ_2 are independent of one another, however, we cannot say a priori what the leading-order term will be. For example, ϵ_1^2 may be larger or smaller than $\epsilon_1\epsilon_2$. However, we can say that the terms retained in Eq. (21), which are $\mathcal{O}(\epsilon_1\epsilon_2)$, are the lowest order terms which describe the influence of the perturbation in the steady geometry on the unsteady flow.

In principle, one could assemble the matrices $[\partial \boldsymbol{b}/\partial \boldsymbol{V}]$, $[\partial \boldsymbol{A}/\partial \boldsymbol{V}]$, etc. in Eq. (20), then multiply by the known perturbations and sum the results to obtain the right-hand side of Eq. (20). However, it is computationally much more efficient to perform the multiplications and summations during the integration phase of the construction of the individual finite elements. Hence, at the element level, we construct $\boldsymbol{A}'$ and $\boldsymbol{b}'$ directly without ever forming the derivative terms. The elemental matrix $\boldsymbol{A}'$ is multiplied by the elemental vector $\boldsymbol{v}$ and the result subtracted from the elemental vector $\boldsymbol{b}'$. Finally, the elemental contributions are assembled to form the global right-hand side to Eq. (21).

As in the steady sensitivity analysis, the computational effort required to solve for $\boldsymbol{v}'$ is insignificant since the matrix $\boldsymbol{A}$ has already

been factored into upper and lower triangular matrices when the nominal unsteady solution v was computed.

Finally, we note that although the present sensitivity analysis has been applied to a finite element discretization of the steady and unsteady full potential equation, the method may be applied equally well to finite difference and finite volume discretizations and may be applied to other flow models (e.g., Euler, Navier–Stokes). The crucial feature which makes the present sensitivity analysis computationally efficient is the use of LU decomposition in the nominal steady and unsteady flow solvers.

Results

Steady Flow Through a Compressor

To demonstrate the present sensitivity analysis, we have analyzed a linear cascade of NACA four digit airfoils. The nominal cascade is similar to modern compressor cascades, and is composed of NACA 5506 airfoils. For the case considered here, the inflow Mach number $M_{-\infty}$ is 0.5, the inflow angle $\beta_{-\infty}$ (measured from the axial direction) is 55 deg, the stagger angle Θ is 45 deg, and the blade-to-blade gap G is 0.9. Figure 2 shows the nominal steady surface pressure P for two different grid resolutions, a 65 × 17 node grid and a 129 × 33 node grid (the pressure has been nondimensionalized by the upstream steady flow quantity $\rho_{-\infty}U^2_{-\infty}$). The flow is entirely subsonic with a maximum Mach number on the suction surface of about 0.61. Note, also, the good agreement between the coarse grid and fine grid solutions.

Having computed the nominal flow through the cascade, we next consider the effect of five different design parameters on the steady flowfield. Two of these parameters are from the NACA four digit airfoil definition: the airfoil thickness and camber. Each of these quantities are measured in fractions of the airfoil chord c. We also consider the effect of changes in the cascade stagger angle Θ, and blade-to-blade gap-to-chord ratio G. Finally, we introduce an additional design variable, the reflex. The reflex parameter modifies the height of the mean line by

$$h_m = rc\sin(2\pi\xi/c) \tag{22}$$

where h_m is the height added to the mean line definition, r is the magnitude of the reflex in fractions of chord, c is the chord, and ξ is the distance along the airfoil chord. The addition of the reflex parameter allows for more complex airfoil shapes.

Figure 3 shows the computed sensitivity of the steady surface pressure to changes in these five geometry variables. The sensitivities are computed using the present sensitivity analysis; all results were computed on a 65 × 17 node grid. To check these results, we also compute the sensitivities using a finite difference approach. The finite-difference result is found by computing the steady flow about two slightly different airfoils, differencing the two solution, and dividing the result by the difference in the airfoil parameter. Note the excellent agreement between the two solutions indicating that the effect of small changes in the design variables is linear and

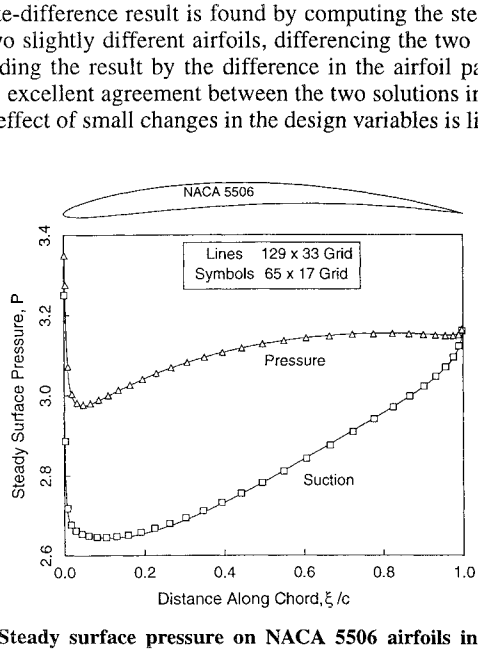

Fig. 2 Steady surface pressure on NACA 5506 airfoils in cascade; $M_{-\infty} = 0.5$, $\beta_{-\infty} = 55$ deg, $\Theta = 45$ deg, $G = 0.9$.

Table 1 Sensitivity of steady forces and moment to perturbations in thickness, camber, stagger, gap, and reflex

Variable	L'	D'	M'_{LE}	L'_y
Thickness	−0.1935	−0.0135	−0.1234	−0.1464
Camber	1.5637	0.1446	−1.4003	1.2080
Stagger	−0.6632	−0.0642	−0.0548	−0.5144
Gap	0.2743	−0.0244	−0.0764	0.1767
Reflex	−1.5506	−0.1476	1.9235	−1.2008

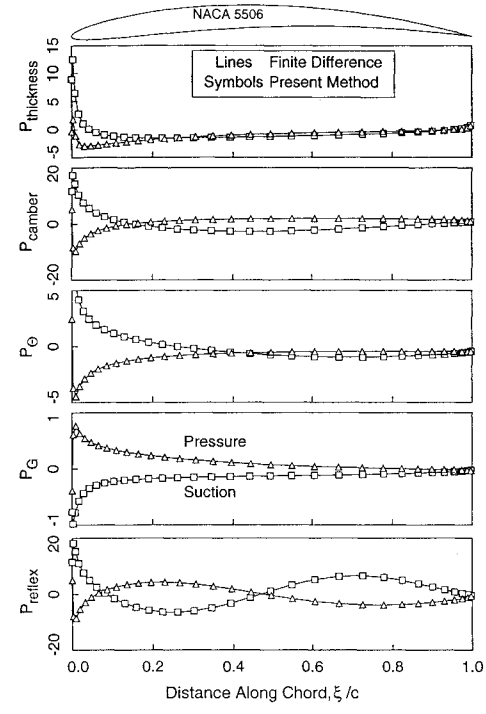

Fig. 3 Sensitivity of steady surface pressure on NACA 5506 airfoils in cascade due to perturbations in thickness, camber, stagger, gap, and reflex.

that the present sensitivity analysis correctly predicts the sensitivities. Also, in all cases, the largest sensitivity in pressure occurs near the leading edge of the airfoil.

Next, the surface pressure sensitivities were integrated to obtain the sensitivity of the steady lift and drag (measured normal to and along the chord) and the moment about the leading edge. These results are given in Table 1. For comparison, the nominal steady lift L is 0.2907, the nominal drag D is −0.0177, the nominal moment about the leading edge M_{LE} is −0.1215, and the nominal lift in the y direction L_y is 0.1931. (The steady lift is normalized by $\rho_{-\infty}U^2_{-\infty}c$, the moment is normalized by $\rho_{-\infty}U^2_{-\infty}c^2$, and lengths are normalized by c.) Also tabulated is the sensitivity of the lift in the y direction L_y (the cascade direction). The steady lift in the y direction is a measure of the turning done by the cascade and, hence, is related to the steady work done by the cascade. Table 1 shows that the lift in the y direction is most sensitive to changes in camber, stagger angle, and reflex. Since these parameters control the metal angle of the trailing edge, and the deviation between the exit flow angle and the metal angle is small for cascades, one would expect these parameters to have a strong influence on the steady lift.

Unsteady Flow Through a Compressor

Having computed the steady flow through the cascade, we next consider the unsteady flow due to plunging and torsional vibration of the airfoils. Figure 4 shows the aerodynamic damping Ξ_B of the cascade vibrating in plunge at three reduced frequencies and for a range of interblade phase angles. For a structurally tuned rotor (i.e., all of the blades have the same structural dynamic properties), the natural modes of the coupled structural/aerodynamic system are traveling waves, each mode corresponding to a different interblade phase angle. The aerodynamic damping of each mode is proportional to the

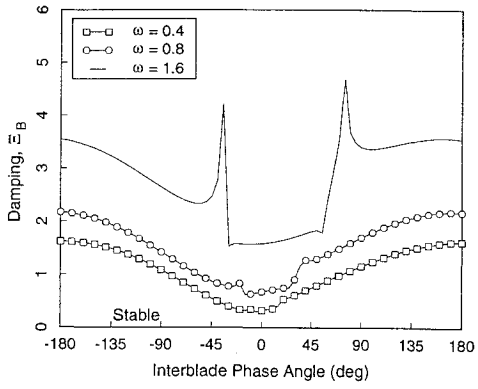

Fig. 4 Aerodynamic damping of cascade of NACA 5506 airfoils vibrating in plunge at reduced frequencies of 0.4, 0.8, and 1.6 for a range of interblade phase angles.

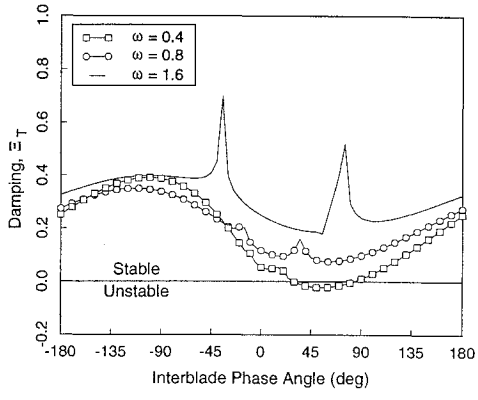

Fig. 5 Aerodynamic damping of cascade of NACA 5506 airfoils pitching about their midchords at reduced frequencies of 0.4, 0.8, and 1.6 for a range of interblade phase angles.

imaginary part of the unsteady lift. Assuming a linear structure with negligible structural damping, the aerodynamic damping determines the aeroelastic stability of the system. Note that for plunging motion, the system in stable, that is, the aerodynamic damping is positive for all interblade phase angles. The aerodynamic damping, however, is generally less for low reduced frequencies (high reduced velocities). The pronounced peaks in the damping curves correspond to acoustic resonances, the interblade phase angles at which acoustic duct modes are "cut on."

Figure 5 shows the aerodynamic damping Ξ_T for the case where the airfoils vibrate in pitch about their midchords (the damping is proportional to the imaginary part of the unsteady moment). Again, the cascade is least stable at the low reduced frequencies. In particular, note that the system is unstable (i.e., $\Xi_T < 0$) for several interblade phase angles at the lowest reduced frequency ω of 0.4.

Consider the case where the airfoils pitch about their midchords with a reduced frequency ω of 0.4 and an interblade phase angle σ of 60 deg (this is the least stable interblade phase angle for the reduced frequency ω of 0.4). Figure 6 shows the imaginary part of the complex amplitude of the nominal unsteady pressure p on the surface of the reference airfoil computed using two different computational grids, a coarse grid containing 65 × 17 nodes, and a fine grid containing 129 × 33 nodes. Note that the coarse and fine grid solutions are nearly identical, although the solutions differ slightly in the leading-edge region on the suction surface. For the case considered here, the imaginary part of the pressure difference across the airfoil is generally negative over the forward-half of the airfoil and positive over the aft-half. Thus, since the airfoil pitches about its midchord (positive nose up), the unsteady pressure does positive aerodynamic work (negative aerodynamic damping) on the airfoil over most of the airfoil.

We next compute the sensitivities of the unsteady surface pressure to changes in geometry. Figure 7 shows the imaginary part of the sensitivity of the unsteady pressure of small changes in six design variables (the reduced frequency ω is included as a design variable

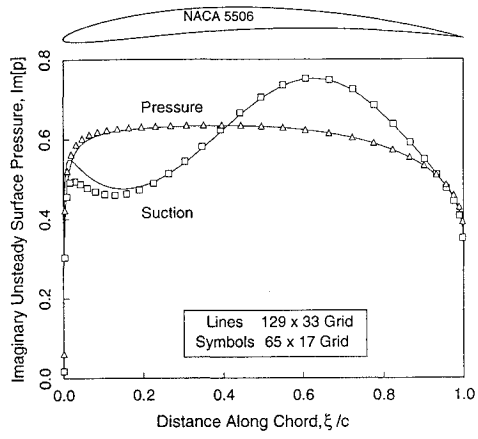

Fig. 6 Imaginary part of unsteady surface pressure of NACA 5506 airfoils pitching about their midchords; ω = 0.4, σ = 60 deg.

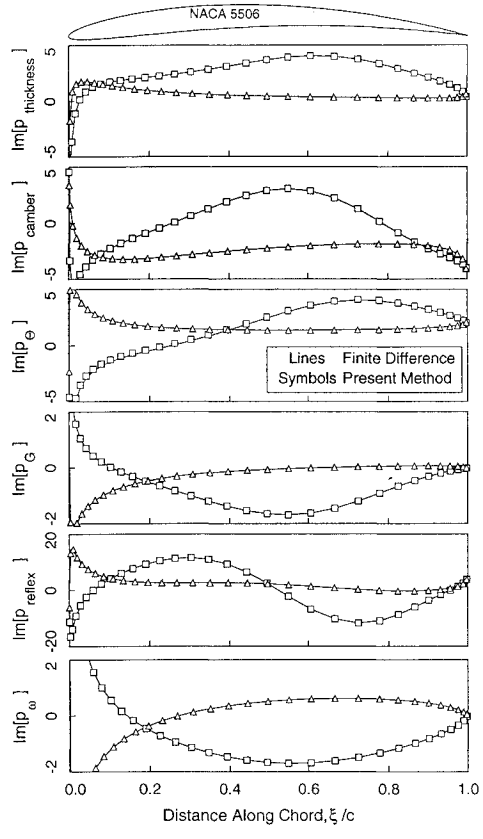

Fig. 7 Imaginary part of sensitivity of unsteady surface pressure of NACA 5006 airfoils pitching about their midchords due to perturbations in thickness, camber, stagger, gap, reflex, and frequency; ω = 0.4, σ = 60 deg.

for unsteady flow calculations). All results were computed on a 65 × 17 node grid. To verify the present method, the sensitivities are also compared to a finite difference calculation. Note the excellent agreement between the two solutions indicating that the present method correctly predicts the sensitivities. Also, the imaginary parts of the sensitivities to changes in stagger and reflex have pressure distributions that are fairly large in magnitude and have distributions that do unsteady work on pitching airfoils. That is, the sensitivity pressure difference across the airfoil changes sign at roughly the midchord of the airfoil.

Having computed the sensitivities of the surface pressure to changes in design variables, we can now integrate to obtain the sensitivities of the aerodynamic damping. Table 2 shows the sensitivity of the aerodynamic damping to small changes in the design variables. The column labeled "Unconstrained" gives the sensitivity of the aerodynamic damping to changes in a single parameter, holding the

Table 2 Sensitivity of aerodynamic damping to perturbations in cascade design variables; $\omega = 0.4$, $\sigma = 60$ deg

	Unconstrained		Constrained	
Variable	Ξ'_T	Ξ'_B	Ξ'_T	Ξ'_B
Thickness	−0.2208	0.3046	0.1344	−0.1879
Camber	−0.0018	−1.9868	−5.2561	3.3668
Stagger	−0.6672	1.4079	——	——
Gap	0.1723	−0.0237	0.2643	−0.1511
Reflex	0.7362	2.0131	——	——
Frequency	0.4030	1.3337	0.4030	1.3337

remaining parameters fixed. Here Ξ'_T is the sensitivity of the aerodynamic damping due to pitching motions, and Ξ'_B is the sensitivity of the aerodynamic damping due to plunging motion. In both cases, the nominal reduced frequency ω is 0.4. Note that, as expected, stagger and reflex have a strong influence on the aerodynamic damping in pitch. Also note that for both pitching and plunging, the sensitivity of the damping to changes in frequency is positive. This result is consistent with the results shown in Figs. 4 and 5.

The results in the unconstrained column of Table 2, however, can be somewhat misleading since changing each design variable independently also changes the steady work done by the blade row and changes the steady incidence at the leading edge of the airfoils. Generally, one would want to leave these quantities unchanged. To avoid this difficultly, it is useful to let two of the design variables "float" so that the steady turning done by the blade row—which is proportional to L_y/G—and the leading-edge incidence angle α remain constant. In this study, we allow the stagger angle Θ and the reflex r to float. For example, then, if we vary the gap G, we must vary the stagger angle and reflex such that

$$\frac{\partial L_y}{\partial \Theta}\Theta' + \frac{\partial L_y}{\partial r}r' + \frac{\partial L_y}{\partial G}G' - \frac{L_y}{G}G' = 0 \tag{23}$$

and

$$\frac{\partial \alpha}{\partial \Theta}\Theta' + \frac{\partial \alpha}{\partial r}r' + \frac{\partial \alpha}{\partial G}G' = 0 \tag{24}$$

Equations (23) and (24) give two equations for the two unknowns Θ' and r' in terms of the known "perturbation" G' and the sensitivities. In Table 2, the column labeled Constrained refers to the sensitivities to each variable computed using this procedure. For both the pitching and plunging cases, it is clear that changing the camber has a very strong effect on the aerodynamic damping. In the pitching case, a (constrained) increase in camber is destabilizing; in the plunging case, an increase in camber is stabilizing.

Redesign of a Compressor for Aeroelastic Stability

Next, we use the constrained sensitivity analysis to redesign an unstable cascade to make it stable. The nominal cascade is the NACA 5506 cascade vibrating in pitch with a reduced frequency ω of 0.4 and an interblade phase angle σ of 60 deg. We note from Table 2 that decreasing the camber has a stabilizing influence on torsional flutter. Thus, for the first redesign (redesign A), we reduce the camber by 0.004 units. Using the constraint relations given above, this requires us to reduce the stagger angle by approximately 1.4 deg and increase the reflex by 0.0064 units. Although the sensitivity analysis predicts that these changes alone will make the airfoil stable, the sensitivity analysis also predicts a large steady pressure gradient on the suction surface near the leading edge. To reduce the pressure gradient, we increase the thickness by 0.02 units, which in turn requires us to reduce the stagger by approximately 0.52 deg and add 0.0014 units of reflex.

For the second redesign (redesign B), we increase the gap-to-chord ratio G to 1.0. Again Table 2 predicts that this change will make the cascade stable, and requires that we reduce the stagger angle by approximately 0.61 deg and 0.0017 units of reflex.

Figure 8 shows the computed steady surface pressure on the redesigned airfoils (c.f. Fig. 2). Also shown in the pressure predicted by the linear sensitivity analysis. The good agreement between the two indicates that nonlinear geometrical effects are small, i.e., terms

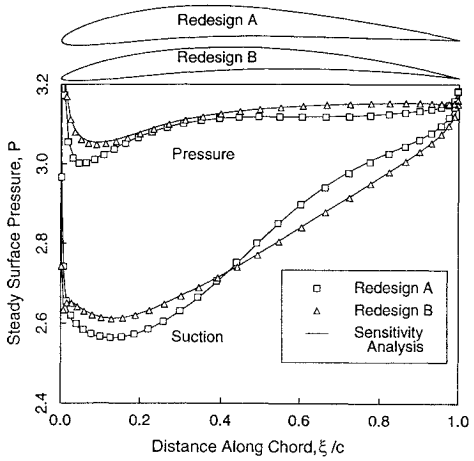

Fig. 8 Steady surface pressure of airfoils of redesigned cascades.

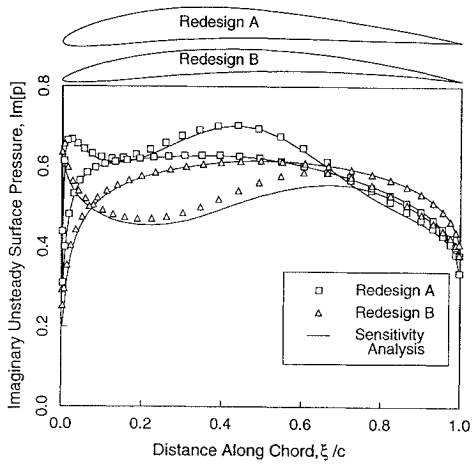

Fig. 9 Real and imaginary parts of unsteady surface pressure on redesigned airfoils pitching about their midchords; $\omega = 0.4$, $\sigma = 60$ deg.

that are $\mathcal{O}(\epsilon_2^2)$ are not important. Note that the steady pressure distribution of the redesigned cascades is significantly different from that of the nominal cascade. In particular, the pressure gradient on the suction surface is larger for both redesigned cascades. Both redesigns are, therefore, likely to increase somewhat the aerodynamic losses of the cascade.

Figure 9 shows the imaginary part of the unsteady pressure on the surface of the redesigned airfoils (c.f. Fig. 6). The unsteady pressure distribution is significantly different than that of the nominal cascade, particularly on the suction surface. Note that the agreement between the sensitivity analysis prediction and the actual pressure distribution for the redesigned cascades, although not quite as good as in the steady case, is still remarkably good indicating that higher order terms [terms which are $\mathcal{O}(\epsilon_1\epsilon_2^2)$] may reasonably be neglected. The actual aerodynamic damping of the redesign A cascade is 0.0086, indicating that the new cascade is stable. The aerodynamic damping of the redesign B cascade is 0.0015, so this cascade is also stable.

Figure 10 shows the aerodynamic damping of the redesigned airfoils for a reduced frequency ω of 0.4 for a range of interblade phase angles σ (c.f. Fig. 5). Note that both redesigned airfoils are stable for all interblade phase angles. Also, the estimates of the aerodynamic damping based on the sensitivity analysis are in very good agreement with the actual damping of the airfoils, again indicating that for moderate changes in the airfoil geometry, nonlinear effects may be neglected.

Computational Efficiency

Finally, a note about computational times. We ran a number of calculations using a 129 × 33 node computational grid on a Silicon Graphics Indigo R4000 workstation. The CPU time required

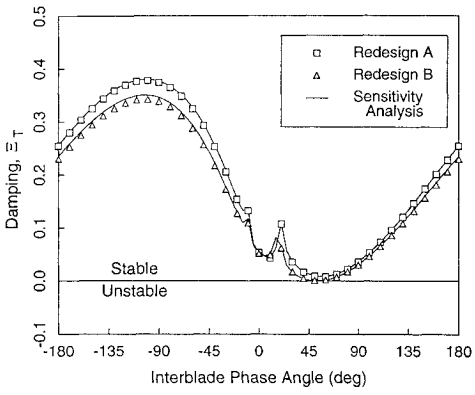

Fig. 10 Aerodynamic damping of cascade of redesigned airfoils pitching about their midchords at a reduced frequency of 0.4 for a range of interblade phase angles.

to compute a single nominal solution was about 30.8 s (23.6 s for the steady flow, 7.2 s for the unsteady flow at a single frequency and interblade phase angle). The present sensitivity analysis with five steady and six unsteady design variables required just 39.3 s (3.9 s for the steady flow, 35.4 s for the unsteady flow). By way of comparison, the finite difference sensitivity analysis took 322.4 s, nearly an order of magnitude more computational time (236.0 s for the steady flow, 86.4 s for the unsteady flow). Furthermore, the present sensitivity analysis, unlike the finite difference analysis, is not susceptible to truncation and round-off errors.

Conclusions

In this paper, a new method is presented for calculating the sensitivity of steady and unsteady flows in cascades to small changes in airfoil and cascade geometry. First, the steady and small disturbance unsteady flow through the cascade is modeled using the steady and small unsteady disturbance versions of the full potential equation. A variational finite element technique is used to discretize the steady and small disturbance unsteady potential equations. Newton iteration is used to solve the steady equations with LU decomposition used at each step; the small disturbance equations are linear and solved with a single LU decomposition.

The sensitivities of the steady and unsteady flowfields to changes in geometry are computed by perturbing the finite element scheme about the nominal solution. The resulting matrix equations for the steady and unsteady sensitivity solutions have similar forms to the nominal flow equations. In fact, the matrix equations to be solved have matrices that are identical to those in the nominal flow solvers. Thus, once the nominal flows have been computed, the sensitivity analysis requires very little additional computer time. Furthermore, the method is general and can also be applied to finite difference and finite volume calculations so long as the nominal flow solvers use LU decomposition.

Finally, we have demonstrated that the sensitivity analysis may be used to guide in the aeroelastic redesign of airfoils. In the example presented in the paper, a cascade that was aeroelastically unstable in torsion was redesigned to be aeroelastically stable.

Acknowledgments

This work was supported by NASA Lewis Research Center, Grant NAG3–1433, with Daniel Hoyniak serving as technical monitor.

References

[1]Verdon, J. M., "Linearized Unsteady Aerodynamic Theory," *AGARD Manual on Aeroelasticity in Axial-Flow Turbomachines, Unsteady Turbomachinery Aerodynamics*, Vol. 1, edited by M. F. Platzer and F. O. Carta, AGARD-AG-298, March 1987, Chap. 2.

[2]Whitehead, D. S., "Classical Two-Dimensional Methods," *AGARD Manual on Aeroelasticity in Axial-Flow Turbomachines, Unsteady Turbomachinery Aerodynamics*, Vol. 1, edited by M. F. Platzer and F. O. Carta, AGARD-AG-298, March 1987, Chap. 3.

[3]Hall, K. C., and Verdon, J. M., "Gust Response Analysis for Cascades Operating in Nonuniform Mean Flows," *AIAA Journal*, Vol. 29, No. 9, 1991, pp. 1463–1471.

[4]Fang, J., and Atassi, H. M., "Numerical Solutions for Unsteady Subsonic Vortical Flows Around Loaded Cascades," *Journal of Turbomachinery*, Vol. 115, No. 4, 1993, pp. 810–816.

[5]Hall, K. C., and Clark, W. S., "Linearized Euler Prediction of Unsteady Aerodynamic Loads in Cascades," *AIAA Journal*, Vol. 31, No. 3, 1993, pp. 540–550.

[6]Holmes, D. G., and Chuang, H. A., "2D Linearized Harmonic Euler Flow Analysis for Flutter and Forced Response," *Unsteady Aerodynamics, Aeroacoustics, and Aeroelasticity of Turbomachines and Propellers*, edited by H. M. Atassi, Springer–Verlag, New York, 1993, pp. 213–230.

[7]Kahl, G., and Klose, A., "Time Linearized Euler Calculations for Unsteady Quasi-3D Cascade Flows," *Unsteady Aerodynamics, Aeroacoustics, and Aeroelasticity of Turbomachines and Propellers*, edited by H. M. Atassi, Springer–Verlag, New York, 1993, pp. 109–126.

[8]Hall, K. C., and Lorence, C. B., "Calculation of Three-Dimensional Unsteady Flows in Turbomachinery Using the Linearized Harmonic Euler Equations," *Journal of Turbomachinery*, Vol. 115, No. 4, 1993, pp. 800–809.

[9]Lighthill, M. J., "A New Method of Two-Dimensional Aerodynamic Design," Aeronautical Research Council, Reports and Memorandum 2112, London, June 1945.

[10]Giles, M. B., and Drela, M., "Two-Dimensional Transonic Aerodynamic Design Method," *AIAA Journal*, Vol. 25, No. 9, 1987, pp. 1199–1206.

[11]Bock, K. W., "Aerodynamic Design by Optimization," *Computational Methods for Aerodynamic Design (Inverse) and Optimization*, AGARD-CP-463, March 1990, Chap. 20.

[12]Jameson, A., "Aerodynamic Design via Control Theory," NASA CR-181749, Nov. 1988.

[13]Ganguli, R., and Chopra, I., "Aeroelastic Optimization of an Advanced Geometry Helicopter Rotor," *AIAA/ASME/ASCE/AHS/ASC Structures, Structural Dynamics and Materials Conference* (Dallas, TX), AIAA, Washington, DC, 1992, pp. 3072–3085 (AIAA Paper 92-2360).

[14]Dodd, A. J., Kadrinka, K. E., Loikkanen, M. J., Rommel, B. A., Sikes, G. D., Strong, R. C., and Tzong, T. J., "Aeroelastic Design Optimization Program," *Journal of Aircraft*, Vol. 27, No. 12, 1990, pp. 1028–1036.

[15]Crawley, E. F., and Hall, K. C., "Optimization and Mechanisms of Mistuning in Cascades," *Journal of Engineering for Gas Turbines and Power*, Vol. 107, No. 2, 1985, pp. 418–426.

[16]Adelman, H. M., and Haftka, R. T., "Sensitivity Analysis of Discrete Structural Systems," *AIAA Journal*, Vol. 24, No. 5, 1986, pp. 823–832.

[17]Haug, E. J., Choi, K. K., and Komkov, V., *Design Sensitivity Analysis of Structural Systems*, Academic, Orlando, FL, 1986.

[18]Taylor, A. C., III, Hou, G. W., and Korivi, V. M., "Methodology for Calculating Aerodynamic Sensitivity Derivatives," *AIAA Journal*, Vol. 30, No. 10, 1992, pp. 2411–2419.

[19]Baysal, O., and Eleshaky, M. E., "Aerodynamic Design Optimization Using Sensitivity Analysis and Computational Fluid Dynamics," *AIAA Journal*, Vol. 30, No. 3, 1992, pp. 718–725.

[20]Sadrehaghighi, I., Smith, R. E., and Tiwari, S. N., "Grid and Design Variables Sensitivity Analyses for NACA Four-Digit Wing-Sections," AIAA Paper 93-0195, Jan. 1993.

[21]Murthy, D. B., and Kaza, K. R. V., "Semianalytical Technique for Sensitivity Analysis of Unsteady Aerodynamic Computations," *Journal of Aircraft*, Vol. 28, No. 8, 1991, pp. 481–488.

[22]Hall, K. C., "Deforming Grid Variational Principle for Unsteady Small Disturbance Flows in Cascades," *AIAA Journal*, Vol. 31, No. 5, 1993, pp. 891–900.

[23]Verdon, J. M., "The Unsteady Flow in the Far Field of an Isolated Blade Row," *Journal of Fluids and Structures*, Vol. 3, March 1989, pp. 123–149.

[24]Bateman, H., "Irrotational Motion of a Compressible Fluid," *Proceedings National Academy of Sciences*, Vol. 16, 1930, pp. 816–825.

[25]Thompson, J. F., Thames, F. C., and Mastin, W., "A Code for Numerical Generation of Boundary-Fitted Curvilinear Coordinate Systems on Fields Containing any Number of Arbitrary Two-Dimensional Bodies," *Journal of Computational Physics*, Vol. 24, No. 3, 1977, pp. 274–302.